Photonic crystal chips for optical interconnects and quantum information processing

Dirk Englund, Andrei Faraon, Ilya Fushman, Bryan Ellis, Hatice Altug, and Jelena Vučković

Ginzton Laboratory, Stanford University, Stanford, CA 94305

ABSTRACT

We have recently demonstrated a number of functional photonic crystals devices and circuits, including an ultrafast, room-temperature, low threshold, nanocavity laser with the direct modulation speed approaching 1THz, an all-optical switch controlled with 60 fJ pulses and with the speed exceeding 20GHz, and a local, reversible tuning of individual quantum dots on a photonic crystal chip by up to 1.8nm, which was then used to tune single quantum dots into strong coupling with a photonic crystal cavity and to achieve a giant optical nonlinearity.

Keywords: quantum information, photonic crystal, quantum dot, optical communications, laser, modulator

1. INTRODUCTION

Photonic crystals enable small-volume, high-Q cavities that enhance the spontaneous emission rate and spontaneous emission coupling efficiency β of embedded emitters. These effects can decrease turn-on time and lasing threshold.[1] Above threshold, higher pump powers lead to faster decay times due to increased stimulated emission rates. Small mode volume PC cavities can be used to achieve large photon densities and speed up this process. Compared to other types of lasers such as VCSELs, PC lasers have lower driving power, increased relaxation oscillation frequency, and potentially faster electrical modulation speed due to lower device capacitance and resistance.

Two considerations are weighed in designing fast photonic crystal lasers: the Q value must be relatively large to achieve SE Purcell enhancement and hence high SE coupling efficiency; at the same time, the cavity ring-down time $\tau_c = Q/\omega$ sets a limit on the response time of the cavity ($\omega = 2\pi/\lambda$ is the resonant frequency). We choose $Q \approx 2 \cdot 10^3$, corresponding to $\tau = 1$ ps. This value of Q is easily achieved with the the single-defect cavity shown in Fig.1(c), defined in a square photonic crystal lattice. The quadrupole mode whose field pattern is shown in the inset, has a $Q \sim 2000$ as predicted by Finite Difference Time Domain (FDTD) simulations.[2]

The single-defect PC laser has the disadvantage that output power is insufficient for most practical applications. A coupled cavity array can overcome this power limitation.[2] The coupled photonic crystal structure achieves very low group velocity in any photonic crystal direction. The 2D coupled cavity array enables even higher output powers while preserving low lasing thresholds. Similarly, coupled x- and y-dipoles modes can also be formed, as shown in Fig.1(a). Though coupled arrays of small numbers of VCSELs were previously investigated,[3,4] coupling between individual lasers is difficult and requires a rather complicated fabrication procedure. Photonic crystal nanocavity arrays allow precise control of both the uniformity and the coupling very precisely.[2] The coupled cavity array and its quadrupole field pattern are shown in Fig.1(a,b). In both modes, the in-plane electric field components E_x and E_y, as well as out-of-plane B_z, are maximized in the center of the slab. This is commonly called the transverse electric (TE)-like mode.

For QD lasers, we used higher Purcell factors with a three-hole defect cavity.[5] Though theoretically limited to $Q \sim 120,000$, the fabricated structure shown in Fig.2 has a quality factor that is diminished to $Q \sim 3000$ because of fabrication imperfections and material loss.[6]

Two modulation schemes are used in telecommunications: small-signal and large-signal modulation.[7,8] In small-signal modulation, the laser is driven at a constant above-threshold pump power $L_{in,0}$ and modulated with a small signal ΔL_{in}, resulting in differential changes ΔP and ΔN_G to the steady-state photon density P_0 and lasing-level carrier densities $N_{G,0}$. In high-β lasers such as the photonic crystal device, strong cavity effects help to increase ω_R without the need to increase pump power, opening a new pathway for increasing laser modulation bandwidth.[9]

In large-signal modulation, the rate equations predict that modulation rate is limited by the pump-level relaxation time $\tau_{E,f}$ and cavity Q. A turn-on delay arises as spontaneous emission builds the cavity field to the point when stimulated

Photonic Crystal Materials and Devices VII, edited by Ali Adibi, Shawn-Yu Lin, Axel Scherer,
Proc. of SPIE Vol. 6901, 69010G, (2008) · 0277-786X/08/$18 · doi: 10.1117/12.774680

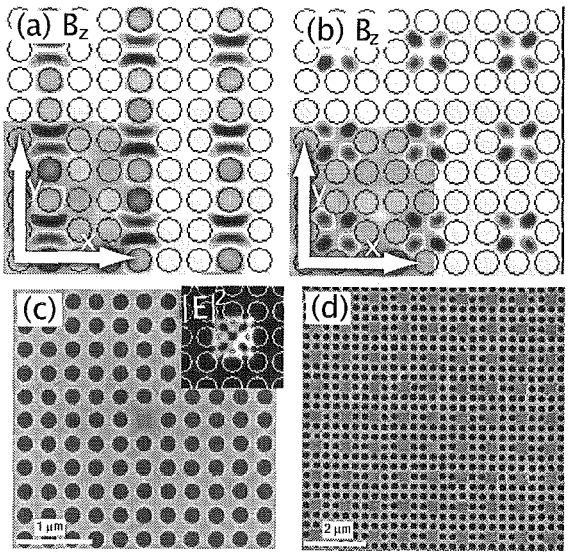

Figure 1. Square-lattice photonic crystal laser structures. (a) x-dipole-mode field pattern (out-of-plane magnetic field B_z). $y-$dipole is rotated by 90°. (b) Quadrupole mode. (c) Single-defect cavity with electric field intensity (inset). (d) Coupled cavity array structure in GaAs.

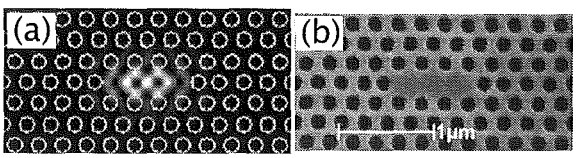

Figure 2. Three-hole defect cavity. (a) FDTD design (left, with electric field intensity) . (b) Fabricated structure in GaAs with central InGaAs QD layer.

emission becomes dominant. This delay time is reduced in the high-Purcell regime through faster SE rate and higher β, as shown in Fig.3. Here the Purcell factor is calculated as

$$F = (0.5) \cdot \frac{3}{4\pi^2} \frac{Q}{V_{mode}/(\lambda/n)^3}, \tag{1}$$

where the factor 0.5 accounts for spatial averaging and is estimated from time-domain Purcell rate measurements.

2. QUANTUM WELL PHOTONIC CRYSTAL LASERS

Quantum wells provide large gain when embedded in the center of the PC cavity, where the resonant TE-like mode has the maximum electric field energy density. To reduce nonradiative (NR) surface recombination on the large QW area exposed through PC patterning, the sample was passivated in a $(NH_4)S$ solution, which resulted in a 3.7-fold reduction in the lasing threshold.[10] We found that surface passivation was critical for room-temperature and continuos-wave (CW) low-temperature operation.

The structures are pumped optically with 3-ps short pulses at an 80MHz repetition rate and a wavelength centered at 750 nm using the confocal microscope as described in.[11] A 75-cm spectrometer is used for high-resolution lasing spectra, while time response is obtained using a streak camera with 3-ps resolution. For higher gain and heat dissipation, we first measured cooled structures which shifts the emission wavelength to 930 nm.[1]

The PC array laser in Fig.1(d) supports a lasing mode at $\lambda_{cav} = 950$ nm at low temperature (LT) of 10K (Fig.4(a)). Fig.4(c) shows the lasing curve for pulsed excitation (3.5 ps at 13 ns repetition), with an average threshold of 6.5 μW(measured before the objective lens). This corresponds to a large peak pump power of $\sim$ 21mW.

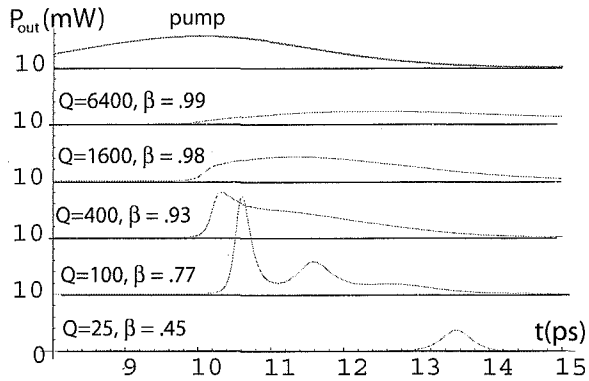

Figure 3. Calculated lasing power $P(t) \cdot (V_{mode}\hbar\omega/\tau_p)$ in response to a 3-ps pump pulse (top), for a range of Q. The turn-on delay drops with increasing Q. The excitation carrier density is $3N_{tr}$ per pulse for all plots, and pump efficiency$\eta = 1$ in this idealized model.

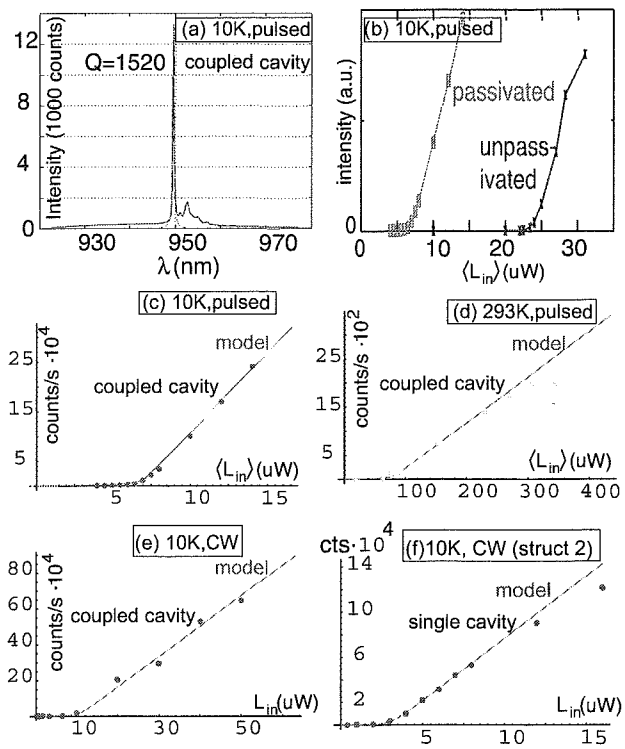

Figure 4. QW-driven PC lasing characteristics (passivated structures). (a) Coupled-cavity array spectrum below threshold and at low temperature (10K). (b) Low-temperature lasing curve shows threshold reduction after passivation. (c,d) Low-and room-temperature lasing curves with pulsed excitation (3.5-pulses at 80MHz repetition, passivated structure). (e,f) Continuous excitation lasing curves for coupled and single cavity. Horizontal axes show average pump power. Fits by a rate equations model.[10]

The threshold power is much lower under continuous pumping at low temperature, as seen in Fig.4(e). For a single cavity, threshold is even lower, near 2μW, shown in Fig.4(f). This threshold and a similarly low value recently reported with GaInAsP/InP QWs[12] are considerably lower than in previous QW lasers.[13,14]

At room temperature, threshold is higher. The lasing curve in Fig.4(d) indicates a threshold of 68 μW average power.[10] Because of faster carrier dynamics, RT operation results in faster modulation speed. This is seen in Fig.5(a) comparing RT and LT lasing response to 3.4-ps-long pump pulses (13 ns repetition).

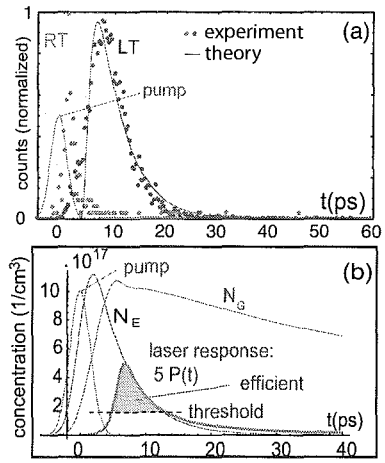

Figure 5. Laser time response. (a) Experimental data shows response nearly following the excitation pulse at room temperature; data at both temperatures are acquired at 2× lasing threshold. (b) Illustration of pump inefficiency in pulsed operation. Pump energy is efficiently channeled into the cavity mode only during lasing (shaded area under $P(t)$ curve, amplified here 5× for visibility); much of the remaining pump energy is wasted to SE and NR losses.

3. QUANTUM DOT PHOTONIC CRYSTAL LASERS

We now shift to PC structures that draw gain from quantum dots instead of quantum wells. QD gain media permit lower threshold due to reduced active area (but also lower saturation power), less nonradiative surface recombination, and greater temperature stability. Their speed is set by the smaller of relaxation rate $1/\tau_{E,f}$ and relaxation oscillation rate ω_R. In ultrasmall, high-Q photonic crystal cavities, the lasing response is sped up through the Purcell effect, while large β and thus higher efficiency and lower threshold are achieved. We investigated these aspects in the 135 nm thick GaAs PC membrane shown in Fig.2(a), containing a high-density (600 μm^{-2}) of InAs QDs.

We measure a gradual onset of lasing near 1μW, as shown in Fig.6(a). From fits to the lasing curve, we estimate a SE coupling factor $\beta \sim 0.2$. Streak camera measurements of the rise time of photoluminescence from quantum dots in bulk GaAs indicate that the carrier relaxation time $\tau_{E,f} \sim 10$ ps for a wide range of pump powers. We also find that resonant pumping of higher-order confined states of the QDs (such as p-level states) does not appreciably lower $\tau_{E,f}$. Because the carrier capture time is longer than the cavity photon lifetime, it ultimately determines the maximum modulation bandwidth. This is what we observe in Fig.6(b) which shows a delay of 13.5 ps (at five times threshold) and does not drop below 12 ps for higher powers. Simulations support this observation as rise time is limited by the carrier capture time. In our cavity-QED-enhanced structure, the relaxation-time limit is rapidly reached in the high-β case. In contrast, in non-PC quantum dot lasers not employing strong cavity effects, far higher pump power is needed to reach this limit.

4. ULTRAFAST CARRIER INDUCED SWITCHING IN PHOTONIC CRYSTAL CAVITIES

The photonic crystal cavity is not only suited for emitting light, but carriers induced inside the cavity can also switch a light beam coupled through the cavity. The induced carriers temporarily change the material's refractive index, which results in a shift the cavity resonance. Such nonlinear optical switching in photonic networks is a promising approach for ultrafast low-power optical data processing and storage. In addition, it might find applications in optical data processing which will be essential for optics-based quantum information processing systems. We observed direct, ultrafast 20 GHz nonlinear

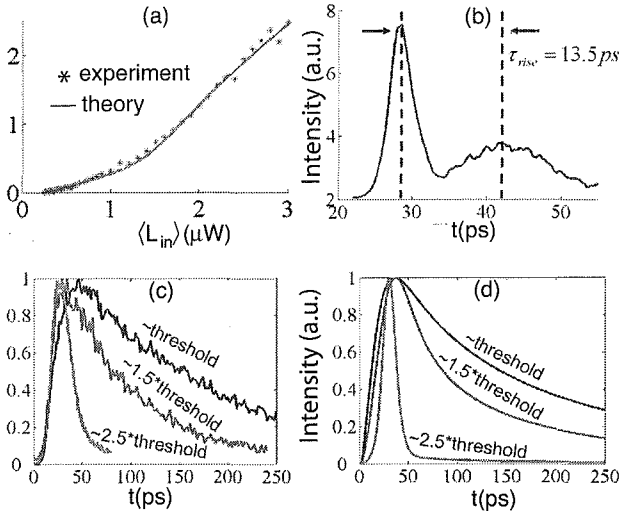

Figure 6. GaAs PC laser with InAs QD gain. (a) Measured lasing curve and fit by a rate equations model. (b) The measured turn-on delay between pump (first peak) and laser response (second peak) is limited by carrier relaxation. (c) Measured large-signal modulation speed increases with pump power. (d) Corresponding fit by rate equations.

optical tuning of photonic crystal PC cavities containing quantum dots QDs.[15] Switching via free-carrier generation is limited by the lifetime of free carriers and depends strongly on the material system and geometry of the device. In our case, the large surface area and small mode volume of the PC reduce the lifetime of free carriers in GaAs.

The experimental data obtained from an L3 cavity are shown in Fig.7. We used moderate energy pulses 120 fJ to shift the cavity by one-half linewidth. Stronger excitation results in higher shifts as indicated by an extremely asymmetric spectrum shown on the inset in (d) of Fig. 3, where 1.4 pJ were used. However, prolonged excitation at this power leads to a sharp reduction in Q over time.

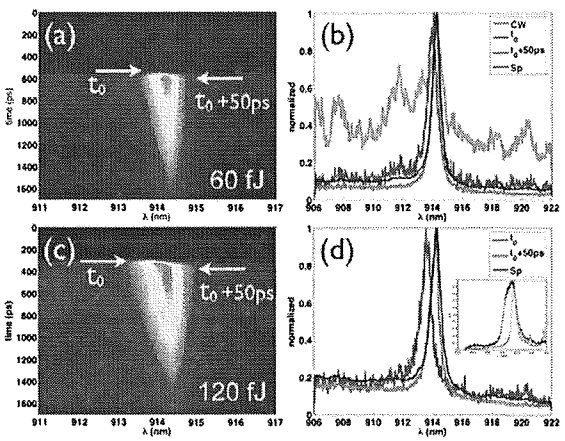

Figure 7. Experimental result of free-carrier cavity tuning. (a,b) Wavelength vs. time plots of the cavity, while the cavity is pumped. (c,d) Normalized spectra of the cavity at different time points from the data (a,b) . In (a), the cavity is always illuminated by a light source and pulsed with a 3 ps Ti:sapphire pulse. Panel (b) shows the normalized cavity spectrum at the peak of the FC distribution t=0 and 50 ps later. We verify that the cavity tunes at the arrival at the pulse by combining the pulsed excitation with a weak cw above-band pump. The emission due to the cw source is always present, and this very weak emission is reproduced in panel (b) as the broad background with a peak at the cold cavity resonace in (b).

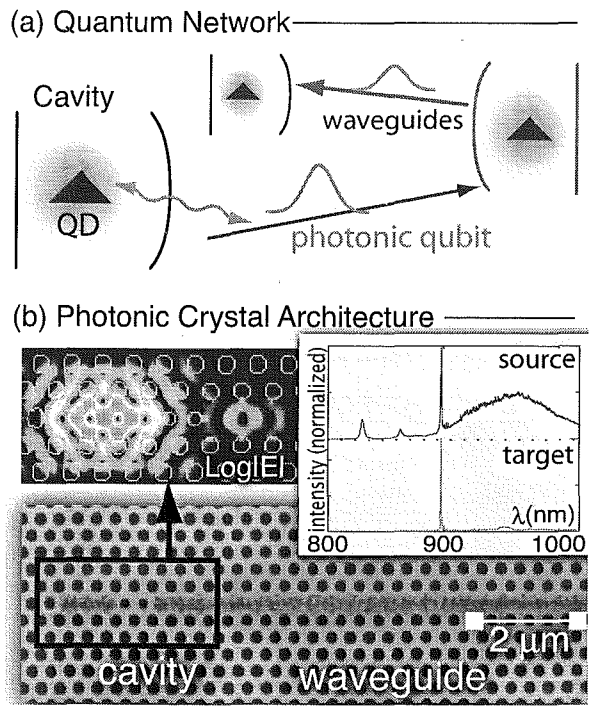

Figure 8. Possible future quantum network on a photonic crystal chip. (a) The cavity-coupled quantum dots would exchange qubits via waveguides. (b) First steps towards on-chip quantum networks. The scanning electron micrograph of a photonic crystal structure combining cavities and waveguides. *Insets:* Electric field intensity and measured spectral filtering of cavity-waveguide-cavity structure.

5. PHOTONIC CRYSTAL QUANTUM NETWORKS

Finally, we address the application of photonic crystals in building quantum information processing devices. The idea of a quantum computer was first proposed by R. Feynman in 1981 as a way to solve intractable quantum mechanical problems.[16] Since then, it has been proven that quantum computers would be inherently far more powerful at solving certain problem than their classical counterparts.[17,18] In addition to computation, cryptography based on quantum systems was proven to offer uncompromised security, relying on the fact that it is impossible to eavesdrop on a transmission without disturbing it.[19,20] The first such quantum cryptography systems have been installed in the past few years. Continued progress, however, requires efficient quantum logic gates. These are essential in a scalable quantum computer that can solve useful problems, and in a quantum repeater that allows secure communication over extended distances.

One of the most promising approaches to quantum information processing is a quantum network which would combine the advantages of photons as information carriers and atomic systems as nonlinear gates and memory.[21] The active medium in our approach consists of InAs quantum dots embedded in a central layer inside the photonic crystal membrane. As opposed to the InAs QD laser samples mentioned above, here the QD density is far lower, less than $100/\mu m^2$, so that single QDs may be addressed inside a photonic crystal cavity.

In recent experiments, we took a first step toward a quantum network with the cavity-waveguide-cavity network illustrated in Fig. 8(b). A QD in the source cavity emits preferentially into the cavity mode,[22] which is then efficiently transferred to the target cavity.[23] Other functions, such as the spectral filtering shown in the inset of Fig.8(b), can be directly integrated into the design.

Many quantum information applications require the QD to emit photons with identical wave packets, requiring high indistinguishability of emitted photons. This indistinguishability can be improved enhancing the QD's spontaneous emission rate above other decoherence mechanisms. We measured 67% wave-function overlap of consecutive photons created in the source cavity.[23]

Most proposals for transferring atomic qubits to photonic qubits require that the QD-cavity coupling outpace other loss mechanisms, such as cavity and QD coupling to the environment. Several groups, including ours, have recently achieved

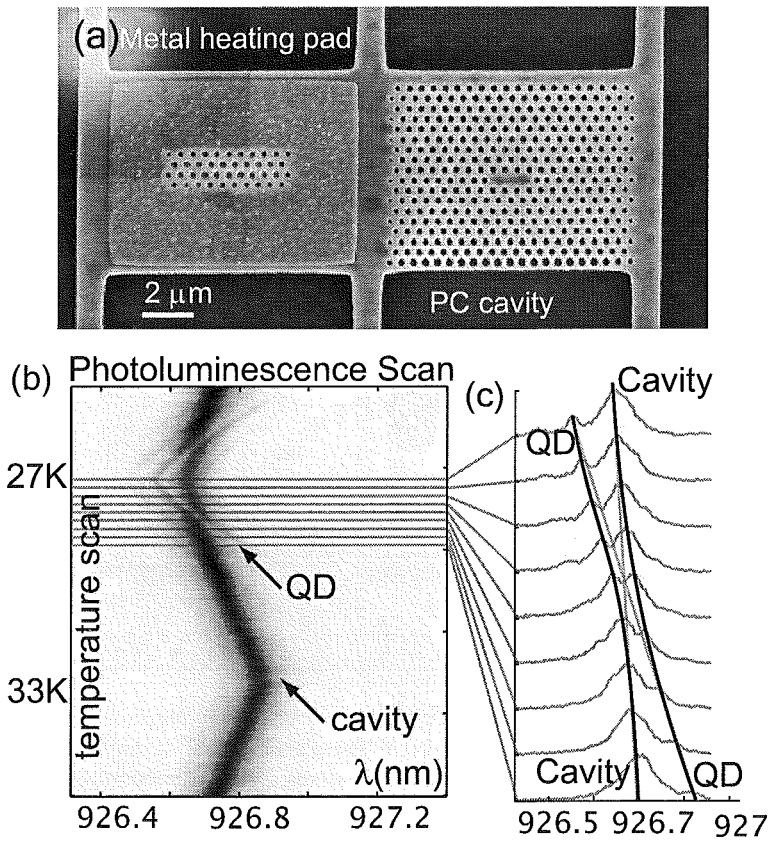

Figure 9. (a) Photonic crystal structure containing cavity and laser heating pad. (b) Spectrum of strongly coupled QD/cavity system tuned through resonance by temperature tuning.[24] (c) Cavity/QD anticrossing. Red lines show QD/cavity tuning if the two were uncoupled.

this regime in solid state systems. In the photoluminescence spectrum of the QD tuned through the cavity (Fig.9((b)), this so-called strong coupling regime results in QD/cavity anticrossing as the QD-like dispersion changes into a cavity-like dispersion (black trace in Fig.9(c)).

We need a set of tools to correct detunings between QDs and cavities in creating a PC quantum network consisting of several QD/cavity nodes. We developed a technique to locally tune the temperature of the QD and cavity using laser heating,[24] using the structure shown in Fig.9(a). In addition, we can tune the resonance wavelength of cavities and waveguides by changing the refractive index of a photoactive film.[25]

We also need a way to directly probe the QD/cavity system by photons. We recently achieved such probing by scattering a weak laser beam off the PC cavity.[26] When the probe beam is resonant with the QD, it destructively interferes with the reflected cavity field in a process analogous to dipole-induced transparency.[27] The resulting reflectivity drop is shown in Fig.10(a). As the probe photon number is increased to roughly one photon per QD lifetime, the transmission dip vanishes. This saturation results in a giant optical nonlinearity which enables strong interaction between only two photons, and is promising for elemental two-qubit quantum gates and potentially classical, all-optical signals processing.

5.1 Acknowledgements

This work has been supported by the MURI Center for photonic quantum information systems (ARO/ARDA Program DAAD19-03-1-0199) and the MARCO IFC Center, NSF Grants ECS-0424080 and ECS-0421483. D.E. was supported by the NDSEG and NSF fellowships, and I.F. by the NDSEG fellowship. We also thank Pierre Petroff and Nick Stoltz of UC Santa Barbara, as well as Yoshihisa Yamamoto and Bingyang Zhang of Stanford University, for quantum dot wafers.

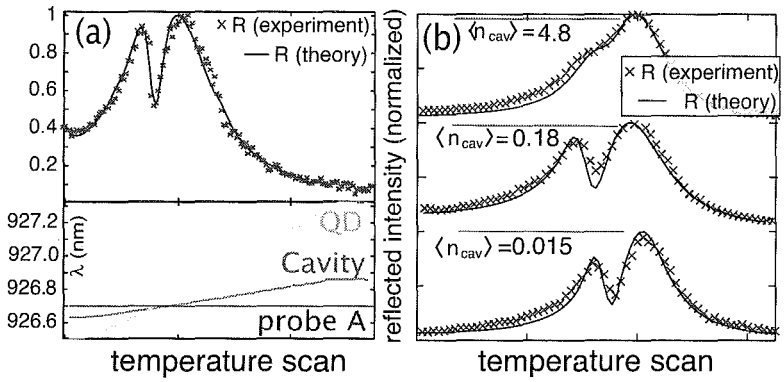

Figure 10. Resonant probing of QD/cavity system. (a) The cavity and quantum dot are scanned across the fixed probe by temperature tuning. The reflected intensity drops when the QD becomes resonant with the probe beam. (b) The QD is saturated at extremely low power, representing a large optical nonlinearity. $\langle n_{cav} \rangle$ denotes the average photon number in the cavity.

REFERENCES

1. H. Altug, D. Englund, and J. Vučković, "Ultrafast photonic crystal nanocavity laser," *Nature Physics* **2**, pp. 484–488, 2006.
2. H. Altug and J. Vuckovic, "Experimental demonstration of the slow group velocity of light in two-dimensional coupled photonic crystal microcavity arrays," *Applied Physics Letters* **86**(11), p. 111102, 2005.
3. D. G. Deppe, J. P. van der Ziel, N. Chand, G. J. Zydzik, and S. N. G. Chu, "Phase-coupled two-dimensional al[sub x]ga[sub 1 - x]as-gaas vertical-cavity surface-emitting laser array," *Applied Physics Letters* **56**(21), pp. 2089–2091, 1990.
4. J. James J. Raftery, A. J. Danner, J. C. Lee, and K. D. Choquette, "Coherent coupling of two-dimensional arrays of defect cavities in photonic crystal vertical cavity surface-emitting lasers," *Applied Physics Letters* **86**(20), p. 201104, 2005.
5. Y. Akahane, T. Asano, B.-S. Song, and S. Noda, "High-Q photonic nanocavity in a two-dimensional photonic crystal," *Nature* **425**, pp. 944–947, Oct. 2003.
6. D. Englund and J. Vučković, "A direct analysis of photonic nanostructures," *Optics Express* **14**, pp. 3472–83, Apr. 2006.
7. L. A. Coldren and S. W. Corzine, *Diode Lasers and Photonic Integrated Circuits*, New York: Wiley, 1995.
8. A. et al., "Injection locking of VCSELs," *J. Sel. Top. Quantum Electron.* **9**, pp. 1386–1393, 2003.
9. G. Bjork and Y. Yamamoto, "Analysis of semiconductor microcavity lasers using rate equations," *IEEE Journal of Quantum Electonics* **27**, pp. 2386–96, Nov. 1991.
10. D. Englund, H. Altug, and J. Vučković, "Low-Threshold Surface-Passivated Photonic Crystal Nanocavity Laser," *Appl. Phys. Lett.* **91**, p. 071124, July 2007.
11. D. Englund, H. Altug, I. Fushman, and J. Vučković, "Efficient Terahertz Room-Temperature Photonic Crystal Nanocavity Laser," *Appl. Phys. Lett.* **91**, p. 071126, July 2007.
12. K. Nozaki, S. Kita, and T. Baba, "Room temperature continuous wave operation and controlled spontaneous emission in ultrasmall photonic crystal nanolaser," *Opt. Express* **15**(12), pp. 7506–7514, 2007.
13. M. Nomura, S. Iwamoto, and M. Nishioka, "Highly efficient optical pumping of photonic crystal nanocavity lasers using cavity resonant excitation," *Appl. Phys. Lett.* **89**(161111), 2006.
14. M. H. Shih, W. Kuang, A. Mock, M. Bagheri, E. H. Hwang, J. O'Brien, and P. Dapkus, "High-quality-factor photonic crystal heterostructure laser," *Appl. Phys. Lett.* **89**(101104), 2006.
15. I. Fushman, E. Waks, D. Englund, N. Stoltz, P. Petroff, and J. Vučković, "Ultrafast nonlinear optical tuning of photonic crystal cavities," *Applied Physics Letters* **90**(9), p. 091118, 2007.
16. R. Feynman, "Simulating Physics with Computers," *International Journal of Theoretical Physics* **21**(6&7), pp. 467–488, 1981.

17. P. Shor, "Algorithms for quantum computation: Discrete log and factoring," *Proceedings of the 35th Annual Symposium on the Foundations of Computer Science* , pp. 124–134, 1994.
18. L. K. Grover, "A fast quantum mechanical algorithm for database search," *8th Annual ACM Symposium on the Theory of Computing (STOC)* , pp. 212–219, 1997.
19. C. Bennett and G. Brassard, "," *Proceedings of IEEE International Conference on Computers, Systems, and Signal Processing, Bangalore, India IEEE, New York* , p. 175, 1984.
20. A. K. Ekert, "Quantum cryptography based on Bell's theorem," *Phys. Rev. Lett.* **67**, pp. 661–663, Aug. 1991.
21. J. I. Cirac, P. Zoller, H. J. Kimble, and H. Mabuchi, "Quantum State Transfer and Entanglement Distribution among Distant Nodes in a Quantum Network," *Physical Review Letters* **78**, pp. 3221–24, Apr. 1997.
22. D. Englund, D. Fattal, E. Waks, G. Solomon, B. Zhang, T. Nakaoka, Y. Arakawa, Y. Yamamoto, and J. Vučković, "Controlling the Spontaneous Emission Rate of Single Quantum Dots in a Two-Dimensional Photonic Crystal," *Physical Review Letters* **95**, p. 013904, July 2005.
23. D. Englund, A. Faraon, B. Zhang, Y. Yamamoto, and J. Vuckovic, "Generation and transfer of single photons on a photonic crystal chip," *Optics Express* **15**, pp. 5550–8, Apr. 2007.
24. A. Faraon, D. Englund, I. Fushman, N. Stoltz, P. Petroff, and J. Vučković, "Local quantum dot tuning on photonic crystal chips," *Appl. Phys. Lett.* **90**, May 2007.
25. A. Faraon, D. Englund, D. Bulla, B. Luther-Davies, B. J. Eggleton, N. Stoltz, P. Petroff, and J. Vučković, "Local tuning of photonic crystal cavities using chalcogenide glasses," *arXiv:0711.0772v2* , Nov. 2007.
26. D. Englund, A. Faraon, I. Fushman, N. Stoltz, P. Petroff, and J. Vučković, "Controlling cavity reflectivity with a single quantum dot," *Nature* **450**(6), pp. 857–61, 2007.
27. E. Waks and J. Vučković, "Dipole induced transparency in frop-filter cavity-waveguide systems," *Physical Review Letters* **96**, April 2006.